Geophysical and Astrophysical Fluid Dynamics,
Vol. 100, No. 1, February 2006, 1–24

Taylor & Francis
Taylor & Francis Group

On the frictional destabilization of abyssal overflows dynamically coupled to internal gravity waves

GORDON E. SWATERS*

Applied Mathematics Institute, Department of Mathematical & Statistical Sciences and
Institute for Geophysical Research, University of Alberta,
Edmonton, Alberta, T6G 2G1 Canada

(*Submitted 11 August 2005; in final form 10 November 2005*)

In the immediate vicinity of a sill, abyssal overflows can possess current speeds greater the local long internal gravity wave speed with bottom friction and downslope gravitational acceleration playing a dominant role in the dynamics. The transition to instability is described of supercritical frictional abyssal overflows on a super-inertial time scale (where rotation, and hence along slope motion, is secondary), but where there is dynamic coupling between the overflow and gravest-mode internal gravity waves in the overlying water column. It is shown that dynamical coupling with ambient internal gravity waves leads to a significant 'up or blue spectrum' shift in the frequencies, wavelengths and growth rates as compared to an instability theory without dynamical coupling. For oceanographically relevant parameter values, the most unstable mode has been found to have a wavelength of about 484 m, an e-folding amplification time of about 13 min, a geostationary period of about 17 min and propagates in a retrograde manner with a co-moving period of about 19 min.

Keywords: Abyssal overflows; Deep western boundary currents; Baroclinic roll waves; Internal gravity waves; Deep water replacement

1. Introduction

The flow of relatively dense water over deep sills is a source point for the development of abyssal currents. These flows, such as the Denmark Strait Overflow (hereafter DSO, e.g., Worthington 1969, Dickson and Brown 1994, Käse and Oschlies 2000, Girton and Sanford 2001, 2003 and Jungclaus *et al.* 2001), make an important global-scale contribution to the convective overturning of the oceans. Abyssal currents of this kind are responsible, although on a smaller scale, for deep water replacement in marginal seas (e.g., LeBlond *et al.* 1991, Karsten *et al.* 1995 and Masson 2002) and the along continental slope propagation of cold bottom-intensified mesoscale anomalies (Houghton *et al.* 1982 and Swaters and Flierl 1991).

*Email: gordon.swaters@ualberta.ca
URL: pacific.math.ualberta.ca/gordon

Geophysical and Astrophysical Fluid Dynamics
ISSN 0309-1929 print: ISSN 1029-0419 online © 2006 Taylor & Francis
http://www.tandf.co.uk/journals
DOI: 10.1080/03091920500489748

Käse *et al*. (2003), analyzing oceanographic data for the DSO region and examining high resolution numerical simulations, describe the differing dynamical regimes between the near-sill and downstream regions. In the downstream region the current is more or less in geostrophic balance and flows, on average, along isobaths. The near-sill overflow is predominately downslope, strongly influenced by bottom friction and is near, and even possibly supercritical with velocities exceeding $1\,\mathrm{m\,s^{-1}}$. Girton and Sanford (2003) argue that the near-sill momentum balance is principally between rotation, downslope gravitational acceleration and bottom friction. This structure can be qualitatively seen in figure 1(a), which shows the depth of the 1.8° potential temperature isotherm (contoured every 500 m) associated with the DSO water as derived from Worthington and Wright (1970) (J. Whitehead, personal communication, 2005). One can see the DSO current descending the sloping bottom into the North Atlantic. In particular, the comparatively pronounced cross-isobath flow of the DSO water between Greenland and Iceland can be seen.

There is considerable temporal and spatial variability associated with overflows (Spall and Price 1998). This variability occurs over a broad range of frequencies and wavelengths. In the sub-inertial regime, abyssal currents can be baroclinically unstable (Swaters 1991, 2005a, Jungclaus *et al*. 2001 and Reszka *et al*. 2002) and can produce mesoscale eddies (Bruce 1995, Krauss and Käse 1998, Swaters 1998, 2005b). In the near-sill region, where the overflow velocities are quite large and geostrophy is no longer the primary dynamical balance, there can be other higher frequency sources for the transition to instability.

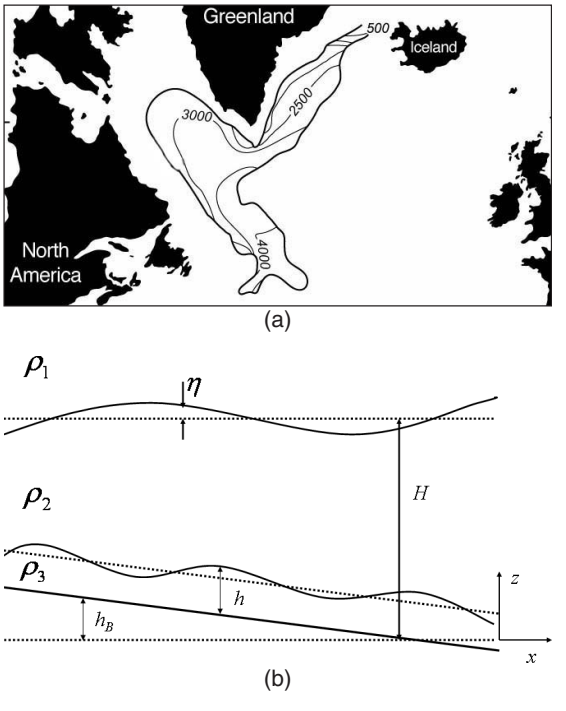

Figure 1. (a) The depth of the 1.8° potential temperature isotherm (contoured every 500 m) associated with the DSO water (J. Whitehead, personal communication, 2005). One can see the DSO current descending the sloping bottom into the North Atlantic. (b) Model geometry used in this article.

Cenedese *et al.* (2004) describe a sequence of laboratory experiments for density-driven abyssal currents flowing down a sloping bottom in a rotating tank. Their investigation showed that over a large range of flow parameters (i.e., rotation rate, density and volume flux of the source and bottom slope) the abyssal current progressed from laminar, to the emergence of 'wave-like disturbances' on the interface between the dense current and the overlying water column to the periodic formation of cyclonic eddies in the overlying water column. In addition, Cenedese *et al.* (2004) presented an analytical solution to the two-layer steady Ekman boundary layer equations on a linearly sloping bottom and determined and described various important sub-limits of the general solution. Cenedese *et al.*'s (2004) experiments showed that the 'wave regime' is associated with the Froude number being greater than one, i.e., the dense current velocity exceeds the local long internal gravity wave speed. Further, Cenedese *et al.* (2004) speculated that the 'wave-like disturbances' were manifestations of a rotational analogue of a roll wave instability. Indeed, this is entirely possible.

Swaters (2003) has shown that in the near-inertial regime, supercritical rotating overflows can be destabilized by bottom friction. Within the overflow, the instabilities take the form of down and along slope propagating, growing periodic bores or pulses (and are the rotational analogues of classical roll waves). For typical oceanographic parameter values, the most unstable mode has a wavelength on the order of about 30 km, propagates prograde with respect to the overflow, has a period, in a geostationary frame of reference, of about 2 h, and an e-folding growth time of about 1 day. This short geostationary period is a consequence of the significant Doppler shift associated with the relatively rapid near-sill overflow current. In a frame of reference moving with the overflow the period is about 7 h. In addition, it was shown that these instabilities can excite long internal gravity waves in the surrounding water column.

However, one unsatisfactory aspect of the Swaters (2003) calculation is that it did not include a full dynamical coupling between the abyssal overflow and the excited internal gravity wave field in the overlying water column. In the near-inertial to slightly sub-inertial regime, the unstable overflow generates an internal wave field in the surrounding ocean, but the wave field makes only a secondary contribution back on the dynamics of the overflow.

Presumably, the dynamic coupling between the internal gravity wave field in the surrounding ocean and the abyssal overflow will modify the stability characteristics. The generation, development and interaction of the internal gravity wave field with abyssal overflows remains poorly understood (Käse *et al.* 2003). These processes are important not only in the interpretation of observations but also in correctly parameterizing abyssal layer mixing processes, particularly those involving gravity waves and bottom friction, in the present generation of ocean general circulation models.

This study continues the examination of the bottom friction induced instability of supercritical abyssal overflows. In contrast to Swaters (2003), here the destabilization process in the super-inertial regime is examined (where rotation, and hence along slope motion, is secondary) but where there is a complete dynamic coupling between the overflow and the surrounding water mass. As in Swaters (2003), this study is focussed on the near-sill region where downslope gravitational acceleration and bottom friction are important and the large current speeds can lead to instability. In particular, the role played by internal gravity waves in the overlying water column in determining the spectral characteristics of unstable overflows is described.

2. Governing equations

The density profile associated with, for example, the DSO (see figure 5 in Girton and Sanford 2003) suggests that, roughly speaking, the water column can be separated into three layers. There is an upper layer about 1000 m thick where the density σ_θ increases linearly from about $27.4\,\mathrm{kg\,m^{-3}}$ (just below the surface mixed layer) to about $27.73\,\mathrm{kg\,m^{-3}}$ (at a depth of about 1000 m), an intermediate layer immediately above the overflow current that is about 500 m thick where the density varies relatively little (average $\sigma_\theta \simeq 27.75\,\mathrm{kg\,m^{-3}}$) and the overflow water (immediately overlying the sloping topography) that is about 300 m thick with a 'substantial' increase in the density (average $\sigma_\theta \simeq 27.83\,\mathrm{kg\,m^{-3}}$). These values imply that characteristic Brunt–Väisälä frequencies (and buoyancy periods) for the overlying ocean and abyssal layer are approximately $1.53 \times 10^{-3}\,\mathrm{s^{-1}}$ (68 min) and $1.87 \times 10^{-3}\,\mathrm{s^{-1}}$ (56 min), respectively.

This stratification profile suggests that it is appropriate to consider a $2\frac{1}{2}$-layer stably stratified abyssal model with variable bottom topography (see figure 1b). The uppermost layer, which is passive and infinitely deep, is denoted as layer 1. The middle, or active upper layer is of finite thickness and is denoted as layer 2. The abyssal layer, i.e., the layer immediately above the bottom topography, is denoted as layer 3.

It is important to emphasize that the analysis presented here is a 'theoretical process study' intended to explore the consequences of frictionally destabilized supercritical abyssal overflows that are dynamically coupled to ambient internal gravity waves and *not* a detailed 'regional modeling study' specially oriented to, for example, the DSO. The description of the stratification and flow characteristics associated with the DSO that have been given above are intended to provide a reasonable physical justification for the model geometry and dynamical processes considered and *not* to assert that the theoretical model examined here accurately models a real oceanographic overflow with its vastly more complex physics and geometry.

In standard notation and with a Boussinesq approximation, the *dimensional* equations of motion are given by (see, e.g., LeBlond and Mysak 1978, Needham and Merkin 1984, Spall and Price 1998)

$$\left(\frac{\partial}{\partial t^*} + u_2^* \frac{\partial}{\partial x^*}\right) u_2^* = -\widetilde{g}\frac{\partial \eta^*}{\partial x^*} + A_H \frac{\partial^2 u_2^*}{\partial x^{*2}}, \tag{1}$$

$$\frac{\partial}{\partial t^*}(\eta^* - h^*) + \frac{\partial}{\partial x^*}\left[u_2^* + \eta^* - h^* - h_B^*\right] = 0, \tag{2}$$

$$\left(\frac{\partial}{\partial t^*} + u_3^* \frac{\partial}{\partial x^*}\right) u_3^* = -\frac{1}{\rho_2}\frac{\partial p^*}{\partial x^*} + \frac{A_H}{h^*}\frac{\partial}{\partial x^*}\left(h^* \frac{\partial u_3^*}{\partial x^*}\right) - \frac{c_D^*}{h^*}\left|u_3^*\right| u_3, \tag{3}$$

$$\frac{\partial h^*}{\partial t^*} + \frac{\partial}{\partial x^*}\left(u_3^* h^*\right) = 0, \tag{4}$$

$$\frac{p^*}{\rho_2} = g'\left(h^* + h_B^*\right) + \widetilde{g}\eta^*, \tag{5}$$

where u_2^*, η^*, u_3^*, p^* and h^* are, respectively, the active upper layer horizontal velocity, the *reduced* upper layer pressure, the abyssal layer velocity, the reduced abyssal layer pressure and the abyssal layer thickness relative to the height of the bottom topography

given by h_B^*. The height of the deforming interface between the passive and active upper layers is given by $H+\eta^*$, where H is a reference (geopotential) height. The reduced gravities $g'=g(\rho_3-\rho_2)/\rho_2>0$ and $\widetilde{g}=g(\rho_2-\rho_1)/\rho_2>0$ where $\rho_1<\rho_2<\rho_3$. The horizontal eddy coefficient is given by A_H and the bottom drag coefficient is given by c_D^*. Implicit in these equations is the assumption that, while the overlying ocean (layers 1 and 2) is stably stratified and has turbulent horizontal mixing, the abyssal layer may be thought of as well mixed but where both bottom friction and turbulent horizontal mixing are present.

The approach taken here to developing the nondimensional equations is to introduce classical reduced-gravity or shallow-water scalings in the abyssal current. The *nondimensional* variables, which do not have an asterisk associated with them, are given by

$$u_2^*=\frac{\widetilde{g}h_*}{\sqrt{g'h_*}}u_2, \qquad \eta^*=h_*\eta, \tag{6}$$

$$u_3^*=\sqrt{g'h_*}u_3, \qquad p^*=\rho_2 g' h_* p, \quad h^*=h_* h, \tag{7}$$

$$h_B^*=s^* L\, h_B(x), \qquad (x^*,t^*)=L\left(x, t/\sqrt{g'h_*}\right), \tag{8}$$

where s^* a representative value for the slope of the bottom topography, h_* is a representative value for the thickness of the abyssal layer, and $L\equiv h_*/s^*$.

Substitution of (6) through to (8) into the dimensional equations (1) through to (5) leads to, for the upper active layer,

$$\left(\frac{\partial}{\partial t}+\delta\gamma^2 u_2\frac{\partial}{\partial x}\right)u_2=-\frac{\partial\eta}{\partial x}+\frac{1}{R_e}\frac{\partial^2 u_2}{\partial x^2}, \tag{9}$$

$$\frac{\partial}{\partial t}(\eta-h)+\gamma^2\frac{\partial}{\partial x}\left\{u_2[1+\delta(\eta-h-h_B)]\right\}=0, \tag{10}$$

and, for the abyssal layer,

$$\left(\frac{\partial}{\partial t}+u_3\frac{\partial}{\partial x}\right)u_3=-\frac{\partial p}{\partial x}+\frac{1}{R_e}\frac{1}{h}\frac{\partial}{\partial x}\left(h\,\frac{\partial u_3}{\partial x}\right)-\frac{c_D}{h}|u_3|u_3, \tag{11}$$

$$\frac{\partial h}{\partial t}+\frac{\partial}{\partial x}(u_3 h)=0, \tag{12}$$

$$p=h+h_B+\delta\gamma^2\eta, \tag{13}$$

where the Reynolds number, R_e, scaled bottom drag coefficient, c_D, and the parameters δ and γ are given by, respectively,

$$R_e\equiv\frac{L\sqrt{g'h_*}}{A_H}, \qquad c_D\equiv\frac{c_D^*}{s^*}, \qquad \delta\equiv\frac{h_*}{H}, \qquad \gamma^2\equiv\frac{\widetilde{g}H}{g'h_*}. \tag{14}$$

The parameter δ, which is the ratio of the abyssal scale thickness to the overall reference mean depth (and must be less than one), is a measure of the magnitude of the dynamical feedback of the upper layer pressure field back onto the lower layer.

As a result of the scaling assumptions made here, δ is also a measure of the degree of nonlinearity in the upper layer dynamics. The parameter γ is the ratio of the scale long internal gravity wave speeds associated with the dynamically active upper layer to the abyssal layer, respectively.

Although there is considerable variability and uncertainty, oceanographically relevant estimates for the order of magnitudes for the parameters are about (see, e.g., Whitehead *et al*. 1990, Karsten *et al*. 1995, Jiang and Garwood 1996, Lane-Serff and Baines 1998, Spall and Price 1998, Etling *et al*. 2000, Jungclaus *et al*. 2001, Reszka *et al*. 2002, Girton and Sanford 2003 and Käse *et al*. 2003)

$$\left.\begin{aligned} c_D^* \approx 0.005, \qquad H \approx 800\,\mathrm{m}, \qquad A_H \approx 25\,\mathrm{m^2\,s^{-1}}, \\ (g', \widetilde{g}) \approx (0.72, 1.77) \times 10^{-3}\,\mathrm{m\,s^{-2}}, \qquad h_* \approx 300\,\mathrm{m}, \qquad s^* \approx 0.02. \end{aligned}\right\} \tag{15}$$

In turn, these would imply

$$\left.\begin{aligned} \sqrt{g' h_*} \approx 46\,\mathrm{cm\,s^{-1}}, \qquad L \approx 15\,\mathrm{km}, \qquad T \approx 9\,\mathrm{h}, \\ c_D \approx 0.25, \qquad \delta \approx 0.38, \qquad \gamma \approx 2.56, \qquad R_e \approx 279. \end{aligned}\right\} \tag{16}$$

3. Stability problem

The steady abyssal flow solutions which perhaps have genuine relevance (Girton and Sanford 2003) *in the near-sill region*, and upon which the theory of classical roll waves has been developed, are the uniform height and velocity, i.e., 'slab', solutions (see, e.g., Jeffreys 1925, Whitham 1974 and Baines 1995) given by

$$u_2 = \eta = 0, \qquad u_3 = U = \frac{1}{\sqrt{c_D}}, \qquad h = 1, \tag{17}$$

on the linearly sloping bottom

$$h_B = -x. \tag{18}$$

These uniform flows are equivalent to the 'stream tube' solutions, without along stream variation, which have been used to examine aspects of the dynamics of rotating turbidity and abyssal currents (e.g., Smith 1975, Killworth 1977, Price and Baringer 1994 and Emms 1998). Perhaps the most unappealing feature of these solutions is that h does not possess groundings. That is, the mean abyssal height does not vanish outside some region with respect to the cross-slope coordinate, the boundary of which corresponds to an intersection of h and the bottom. The model developed by Swaters (1991) (see, also, Swaters 1998, Poulin and Swaters 1999 and Reszka *et al*. 2002) was able to explicitly determine the baroclinic stability characteristics for a grounded abyssal flow. Nevertheless, the stability characteristics described here will be of genuine relevance in understanding the range of dynamics possible in the transition to instability for abyssal overflows, even if it is not possible to immediately apply these results to a specific situation.

Substitution of the perturbed solution

$$(u_2, \eta, u_3, h) \simeq \left(0, 0, \frac{1}{\sqrt{c_D}}, 1\right) + \left(\widetilde{u}_2, \widetilde{\eta}, \widetilde{u}_3, \widetilde{h}\right), \tag{19}$$

into (2.9) through to (2.13), leads to the linear stability problem, after dropping the tildes and a little algebra,

$$\left(\frac{\partial}{\partial t} - \frac{1}{R_e}\frac{\partial^2}{\partial x^2}\right)\frac{\partial}{\partial t}(\eta - h) - \gamma^2(1-\delta)\frac{\partial^2 \eta}{\partial x^2} = 0, \tag{20}$$

$$\left[\left(\frac{\partial}{\partial t} + \frac{1}{\sqrt{c_D}}\partial_x\right)^2 - \frac{\partial^2}{\partial x^2} + \frac{\partial}{\partial x} + \left(2\sqrt{c_D} - R_e^{-1}\frac{\partial^2}{\partial x^2}\right)\left(\frac{\partial}{\partial t} + \frac{1}{\sqrt{c_D}}\frac{\partial}{\partial x}\right)\right]h - \delta\gamma^2\frac{\partial^2 \eta}{\partial x^2} = 0, \tag{21}$$

with the auxiliary relations

$$\frac{\partial}{\partial x}u_3 = -\left(\frac{\partial}{\partial t} + \frac{1}{\sqrt{c_D}}\frac{\partial}{\partial x}\right)h, \quad \left(\frac{\partial}{\partial t} - \frac{1}{R_e}\frac{\partial^2}{\partial x^2}\right)u_2 = -\frac{\partial \eta}{\partial x}, \quad p = h + \delta\gamma^2\eta.$$

Note that the spatially varying $O(\delta h_B)$ terms in (20) have been neglected. A WKB analysis (not presented here) shows that this approximation will have a quantitative but not a qualitative impact on the results described here. The primary effect of this term would be to introduce a spatially slowly decaying structure in the perturbation fields in the downslope direction due to the increase in mean depth and continuity in mass flux. (Retaining the linear variation in mean depth would imply that the kernel of the separated spatial operator in (20) would be given by ordinary Bessel functions of order zero which decay proportional to the square root of their argument.) Neglecting these terms in (20) allows simple normal mode solutions to the stability problem. Notwithstanding this rationale, it is worth pointing out that this geometrical effect may have a role to play in localizing the variability associated with the transition to instability described here to the immediate near-sill region.

Assuming a normal mode solution of the form (with the pure viscous mode factored out of the complex-valued growth rate)

$$(h, \eta) = \left(\widetilde{h}, \widetilde{\eta}\right)\exp\left[\mathrm{i}kx + \left(\sigma - \frac{k^2}{2R_e}\right)t\right] + c.c., \tag{22}$$

where *c.c.* means the complex conjugate of the preceding term, leads to the algebraic system, after dropping the tildes,

$$\mathcal{M}(h, \eta)^{\top} = \mathbf{0},$$

where

$$\mathcal{M} = \begin{bmatrix} \sigma^2 - \left(\dfrac{k^2}{2R_e}\right)^2 & -\left[\sigma^2 + \gamma^2 k^2(1-\delta) - \left(\dfrac{k^2}{2R_e}\right)^2\right] \\ (\sigma - \sigma_+)(\sigma - \sigma_-) & \delta\gamma^2 k^2 \end{bmatrix},$$

with

$$\sigma_{\pm} \equiv -\left(\frac{ik}{\sqrt{c_D}} + \sqrt{c_D}\right) \pm \sqrt{\left(\sqrt{c_D} + \frac{k^2}{2R_e}\right)^2 - (ik + k^2)}, \tag{23}$$

where the branch cut is taken along the negative real axis. For a nontrivial solution, $\det(\mathcal{M}) = 0$, which yields the quartic in σ given by,

$$(\sigma - \sigma_+)(\sigma - \sigma_-)\left[\sigma^2 + \gamma^2 k^2(1-\delta) - \left(\frac{k^2}{2R_e}\right)^2\right] + \delta\gamma^2 k^2\left[\sigma^2 - \left(\frac{k^2}{2R_e}\right)^2\right] = 0, \tag{24}$$

giving rise to solutions of the form $\sigma = \sigma(k, c_D, \delta, R_e, \gamma)$.

The limit where the abyssal flow is no longer *dynamically* coupled to the overlying layer, but the abyssal layer can still passively excite motion in the upper layer, corresponds to $\delta = 0$, and the dispersion relation governing the *instability* (within the abyssal overflow) reduces to $\sigma = \sigma_{\pm}$. The additional $\delta = 0$ roots, given by

$$\sigma = \pm ik\sqrt{\gamma^2 - [k/(2R_e)]^2},$$

correspond to *dissipating* free internal gravity waves in the overlying ocean (i.e., homogeneous solutions for η (see 20) in the uncoupled limit). Swaters (2003) has described the stability characteristics of the $\delta \to 0$ limit when rotation is included and where the upper layer is inviscid and continuously stratified.

In the $\delta \to 0$ limit, and as determined from (22) and (23), a mode with a given wave number k will be stable provided

$$\mathrm{Re}(\sigma_+) \le k^2/(2R_e),$$

i.e.,

$$\mathrm{Re}\left(\sqrt{\left(\sqrt{c_D} + \frac{k^2}{2R_e}\right)^2 - (ik + k^2)}\right) \le \sqrt{c_D} + \frac{k^2}{2R_e}.$$

This can be considerably simplified by introducing the Euler decomposition

$$\alpha \exp(\mathrm{i}\beta) = \left(\sqrt{c_D} + \frac{k^2}{2R_e}\right)^2 - k^2 - ik,$$

(which serves to define the real numbers α and β) allowing the above stability condition to be re-written in the form

$$\alpha[1 + \cos(\beta)] \le 2\left(\sqrt{c_D} + \frac{k^2}{2R_e}\right)^2,$$

or, equivalently, after substituting in for α and β

$$\left[\left(\sqrt{c_D}+\frac{k^2}{2R_e}\right)^2-k^2\right]^2+k^2\le\left[\left(\sqrt{c_D}+\frac{k^2}{2R_e}\right)^2+k^2\right]^2,$$

from which it follows that stability occurs *if and only if* (for $k\neq 0$, the flow is unconditionally stable for $k=0$)

$$\sqrt{c_D}+\frac{k^2}{2R_e}\ge\frac{1}{2}. \tag{25}$$

Thus, frictional downslope abyssal overflows will be stable on a sufficiently gentle slope, or when the bottom drag coefficient is large enough (recall $c_D=c_D^*/s^*$).

Moreover, in the uncoupled, inviscid $R_e\to\infty$ limit, (25) implies

$$c_D\ge\tfrac{1}{4}\Longleftrightarrow\text{stability}, \tag{26}$$

or, equivalently, written in terms of the Froude number, instability necessarily occurs when

$$F\equiv\frac{U^*}{\sqrt{g'h_*}}>2,\quad\text{where } U^*=\sqrt{\frac{s^*g'h_*}{c_D^*}}, \tag{27}$$

which is just the classical roll wave stability result (see, e.g., Jeffreys 1925, Whitham 1974 and Baines 1995).

A physical description of 'roll wave destabilization' is given by Baines (section 2.3.4, 1995) within the reduced gravity context. It does not correspond to the release of potential energy (as in baroclinic instability) or kinetic energy (as in barotropic instability) or Kelvin–Helmholtz (KH) instability (shear flow instability in the presence of gravity). Physically, this transition mechanism occurs because positive (negative) perturbations in the thickness of the abyssal layer leads to diminished (increased) frictional drag and hence accelerates (decelerates) the flow. Mathematically, the instability occurs when the perturbation group velocity lies outside the range of allowed gravity-wave group velocities (information cannot travel faster than the fastest gravity wave in this system). The instability is not a energy conversion process. It corresponds to the onset of 'disorder' in the system (Baines, 1995). As the destabilization continues, advection leads to amplitude steepening and the eventual formation of hydraulic jumps and bores. In the ocean, with its vast array of additional physics this scenario is undoubtedly more complex. Of concern here is how the instability characteristics are modified when dynamic baroclinic coupling occurs.

Note that (25) implies the existence of a high wave number cutoff if R_e is finite. Indeed, if R_e was infinite, then the instability problem exhibits an ultraviolet catastrophe, i.e., the most unstable mode has an infinite wave number in both the $\delta=0$ and $\delta\neq 0$ problems. But this is outside the *a priori* assumptions upon which shallow-water theory for the model equations is based.

In the limit $\delta = 1$ (this is actually an unphysical value for δ since it implies that there is no overlying water column, i.e., $h_* = H$, see figure 1b), it follows from (24) that the dispersion relation governing the instability is given by

$$(\sigma - \sigma_+)(\sigma - \sigma_-) + \gamma^2 k^2 = 0, \tag{28}$$

giving rise to the solutions

$$\begin{aligned}\sigma &= \frac{\sigma_+ + \sigma_- \pm \sqrt{(\sigma_+ - \sigma_-)^2 - 4\gamma^2 k^2}}{2} \\ &= -\left(\frac{\mathrm{i}k}{\sqrt{c_D}} + \sqrt{c_D}\right) \pm \sqrt{\left(\sqrt{c_D} + \frac{k^2}{2R_e}\right)^2 - \mathrm{i}k - (1+\gamma^2)k^2}.\end{aligned} \tag{29}$$

Note that (29) is identical to (23) if $\gamma = 0$.

It follows from (29) and (22) that, in the $\delta = 1$ limit, a mode with a given wave number k will be stable, again, provided

$$\mathrm{Re}\{\sigma\} \leq k^2/(2R_e),$$

which is satisfied (following a similar derivation as that for (25)) *if and only if* (again, for $k \neq 0$, the flow is unconditionally stable for $k = 0$)

$$\sqrt{c_D} + \frac{k^2}{2R_e} \geq \frac{\sqrt{1+\gamma^2}}{2(1+\gamma^2)}, \tag{30}$$

which is, of course, identical to (25) if $\gamma = 0$.

It follows that the instability is *not* eliminated as $\delta \to 1^-$. Irrespective of the fact that $\delta = 1$ is an 'unphysical' limit, it is the solutions (29) that the solutions of (24) approach as $\delta \to 1^-$. For the dispersion relation (28), it follows that $\eta = h$. The additional $\delta = 1$ roots, given by $\sigma = \pm k^2/(2R_e)$, correspond to the non-propagating viscous mode in the overlying ocean (i.e., homogeneous solutions for η (see 20) if $\delta = 1$). Note that on account of (22), the actual maximum growth rate for the viscous mode is always zero.

4. Stability characteristics

Since this article is principally focussed in describing the instability when the overflow is dynamically coupled to internal gravity waves, it is useful to *very briefly* summarize the principal stability characteristics in the uncoupled $\delta = 0$ limit. In this limit, the instability is fully determined by the dynamics of the overflow alone and the dispersion relation (24) reduces to simply $\sigma = \sigma_\pm$. The internal gravity wave field that arises in the overlying water column is 'passively' forced and does not make any dynamical feedback on the overflow (there are no η terms in the abyssal layer equations).

For the remainder of this section, it is convenient to work with the *total complex-valued growth rate*, denoted as $\widetilde{\sigma}$, and given by (see (22)),

$$\widetilde{\sigma} \equiv \sigma - \frac{k^2}{2R_e},$$

and where, for convenience, the tilde will be subsequently dropped.

Figure 2(a) is a plot of the wave number of the most unstable mode (denoted as $k_{\max}$) *versus* c_D for $\delta = 0$ and $R_e = 279$. The phrase 'most unstable mode' (denoted as $\sigma_{\max}$) means the mode with the largest value of $\mathrm{Re}\{\sigma\}$ when considered as a function of the wave number k, for a given value of the other parameters (in the $\delta = 0$ case the only other parameters are c_D and R_e since γ does not appear in $\sigma_{\pm}$). When instability occurs, the most unstable mode always occurs at the wave number $k = k_{\max}$ satisfying

$$\left.\frac{\partial \mathrm{Re}\{\sigma\}}{\partial k}\right|_{k=k_{\max}} = 0, \quad \sigma_{\max} \equiv \sigma|_{k=k_{\max}}. \tag{31}$$

The wave number of the most unstable mode monotonically decreases as c_D increases until $c_D = 0.25$ is reached. After this point, the most unstable mode occurs at $k_{\max} = 0$ (which is neutrally stable; all other modes exponentially decay in time due to horizontal friction). Since there is no finite steady overflow solution when $c_D = 0$ (see (17)), the stability problem is not continuous at the boundary point $c_D \to 0^+$. The singular nature of the value $c_D = 0$ is indicated with an open circle at that limit point.

Figure 2(a) suggests that $k_{\max} \simeq 2$ is a 'typical' value for the wave number over much of the $c_D < 0.25$ unstable region. Since the length scale is 15 km, $k_{\max} \simeq 2$ corresponds to a wavelength of about 45 km. As will be shown, when dynamical coupling between the overflow and internal gravity waves is included there will be a significant shortening of the wavelength of the most unstable mode.

Figure 2(b) is a plot of the growth rate of the most unstable mode (denoted as $\mathrm{Re}\{\sigma_{\max}\}$) *versus* c_D for $\delta = 0$ and $R_e = 279$. The growth rate of the most unstable mode monotonically decreases as c_D increases until $c_D = 0.25$ is reached. After this point, the most unstable mode is neutrally stable (i.e., $\mathrm{Re}\{\sigma_{\max}\} = 0$). A typical value for $\mathrm{Re}\{\sigma_{\max}\}$ when instability occurs is about 0.2. Since the time scale is about 9 h, $\mathrm{Re}\{\sigma_{\max}\} \simeq 0.2$ corresponds to an e-folding amplification time of about 45 h. As will be shown, when internal gravity wave coupling is taken into account, the growth rates will become much higher so that the e-folding amplification will be much faster.

Figure 2(c) is a plot of the (geostationary) frequency of the most unstable mode, denoted as $\omega_{\max}$, and determined by

$$\omega_{\max} \equiv -\mathrm{Im}\{\sigma_{\max}\}, \tag{32}$$

versus c_D for $\delta = 0$ and $R_e = 279$. The frequency of the most unstable mode is positive and monotonically decreases as c_D increases until the stability boundary $c_D = 0.25$ is reached. For $c_D \geq 0.25$, $\omega_{\max} = 0$. Note that $\omega_{\max} \to \infty$ as $c_D \to 0^+$. The *geostationary* frequency becomes unbounded as $c_D \to 0^+$ because the speed of the mean abyssal current (given by $U = 1/\sqrt{c_D}$) becomes unbounded as the bottom friction parameter goes to zero (see (18)) and thus the Doppler frequency shift,

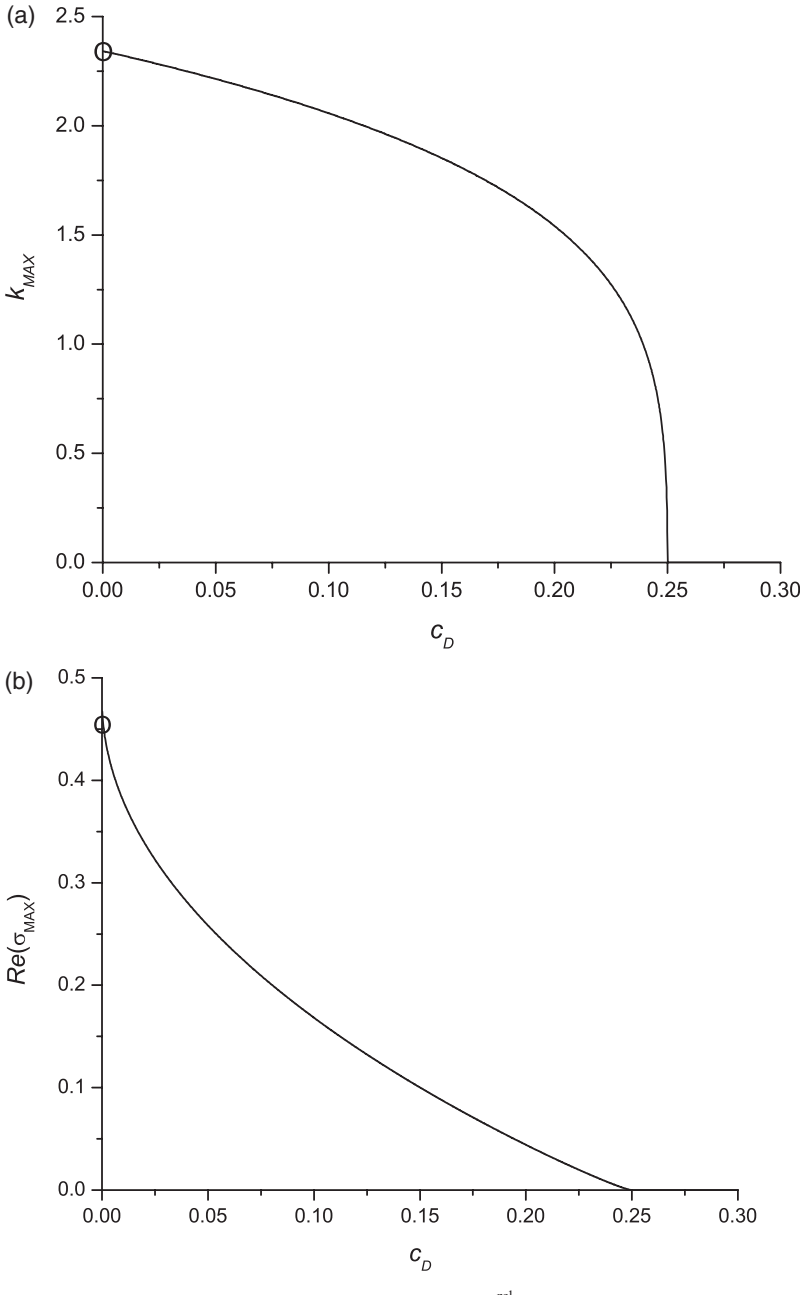

Figure 2. (a) $k_{\max}$, (b) $\mathrm{Re}\{\sigma_{\max}\}$, (c) $\omega_{\max}$ and (d) $\omega_{\max}^{\mathrm{rel}}$, respectively, *vs.* c_D for $\delta = 0$.

given by $k_{\max}/\sqrt{c_D}$, becomes unbounded as well. A typical value for $\omega_{\max}$ when instability occurs is about 10, which corresponds to a period of about 6 h. When internal gravity wave coupling is taken in account, the period of the most unstable mode will be reduced significantly.

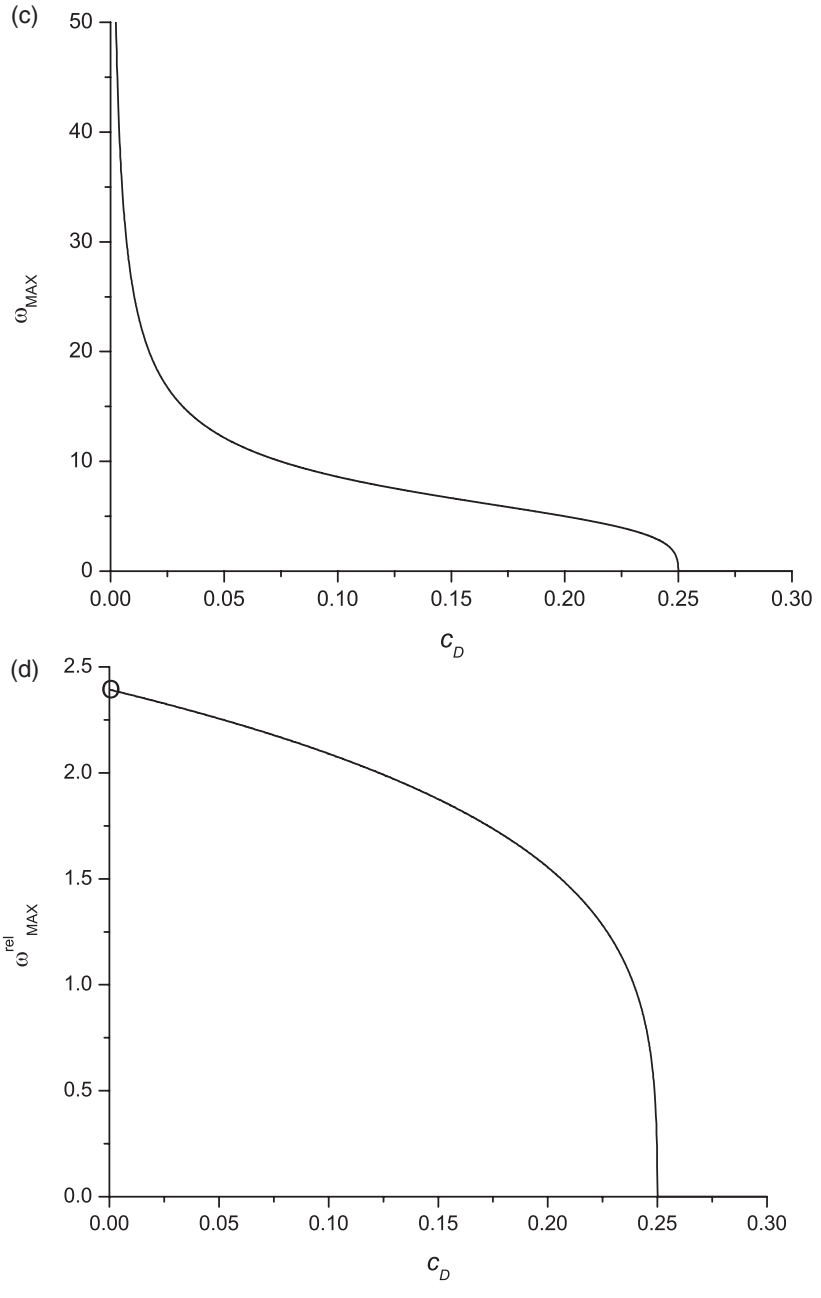

Figure 2. Continued.

Figure 2(d) is a plot of the *relative* frequency of the most unstable mode (i.e., in a frame of reference moving with the mean flow), denoted as $\omega^{\mathrm{rel}}_{\mathrm{max}}$, and determined by

$$\omega^{\mathrm{rel}}_{\mathrm{max}} \equiv -\mathrm{Im}(\sigma_{\mathrm{max}}) - k_{\mathrm{max}}/\sqrt{c_D}, \tag{33}$$

versus c_D for $\delta = 0$ and $R_e = 279$. The dramatic effect of the Doppler shift in the frequency associated with the mean flow can be seen when $\omega_{\max}$ in figure 2(c) is compared with $\omega_{\max}^{\text{rel}}$ in figure 2(d). The relative frequency of the most unstable mode is always positive and monotonically decreases as c_D increases until the stability boundary $c_D = 0.25$ is reached. For $c_D \geq 0.25$, $\omega_{\max}^{\text{rel}} = 0$.

The fact that $\omega_{\max}^{\text{rel}} > 0$ when instability occurs implies that the most unstable modes propagate prograde with respect to the mean abyssal current. It will be shown that when the instability is fully coupled to an internal gravity wave field in the overlying water column, the most unstable modes no longer necessarily propagate prograde with respect to the mean abyssal overflow and indeed, generically, the propagation characteristics are retrograde.

In summary, when $\delta = 0$, that is, when there is no dynamic coupling with an internal gravity wave field, and with $R_e = 279$, the most unstable mode has a wavelength of about 45 km, a period of about 6 h and an e-folding amplification time of about 45 h. Swaters (2003) describes how these stability characteristics are modified when rotation is included and when both downslope and cross-slope motion is allowed. Generally speaking, there is a shift to lower frequencies and wave numbers and the growth rates are decreased. For the remainder of this section attention will be focussed on describing the coupled instability.

Figure 3(a) is a contour plot of the wave number of the most unstable mode $k_{\max}$ in the (c_D, δ)-plane assuming $R_e = 279$ and $\gamma = 2.56$. In the context of figures 3, the 'most unstable mode' is that normal mode with the largest value of $\text{Re}\{\sigma\}$ considered as a function of the wave number k for a given value of all the other parameters c_D, δ, R_e and γ. Comparing figure 3(a) with figure 2(a) a number of important qualitative properties can be seen. First, internal gravity wave coupling leads to significantly higher wave numbers for the most unstable mode. Second, as δ increases from zero, $k_{\max}$ increases initially and then decreases as $\delta \to 1^-$. The maximum value of $k_{\max}$ in figure 3(a) is about 264.85 (corresponding, dimensionally, to a mode with a wavelength of about 356 m) and is located at about $(c_D, \delta) \simeq (0.12, 0.58)$. For the 'typical' (c_D, δ) values of (0.25, 0.38), as determined in (2.16), $k_{\max} \simeq 194.65$ (corresponding, dimensionally, to a mode with a wavelength of about 484 m).

Figure 3(b) is a contour plot of the growth rate of the most unstable mode, given by $\text{Re}\{\sigma_{\max}\}$, in the (c_D, δ)-plane assuming $R_e = 279$ and $\gamma = 2.56$. Comparing figure 3(b) with figure 2(b), the growth rates for the coupled instability are two order of magnitude larger than those for the $\delta = 0$ problem over much of the unstable region for the same value of c_D. As in figure 3(a), the qualitative behavior $\text{Re}\{\sigma_{\max}\}$ corresponds, generally speaking, to increasing growth rates as δ increases initially from zero, with a maximum reached and then decreasing as $\delta \to 1^-$. As mentioned above, the growth rates are not uniformly zero along $\delta = 1$ (but are quite small and are determined by (29)). It follows from (25) and (29) that the high wave number cutoff along $\delta = 0$ is about 16.7 and along $\delta = 1$ it is about 10.07 (for $R_e = 279$ and $\gamma = 2.56$). The maximum growth rate in figure 3(b) is about 106.05 (corresponding, dimensionally, to an e-folding amplification time of about 5 min) and is located at about $(c_D, \delta) \simeq (0.09, 0.55)$. For the 'typical' (c_D, δ) values of (0.25, 0.38), as determined in (16), $\text{Re}\{\sigma_{\max}\} \simeq 42.66$ (corresponding, dimensionally, to an e-folding amplification time of about 13 min). This is a substantially more rapid time scale for the destabilization than the uncoupled rotating instability described by Swaters (2003).

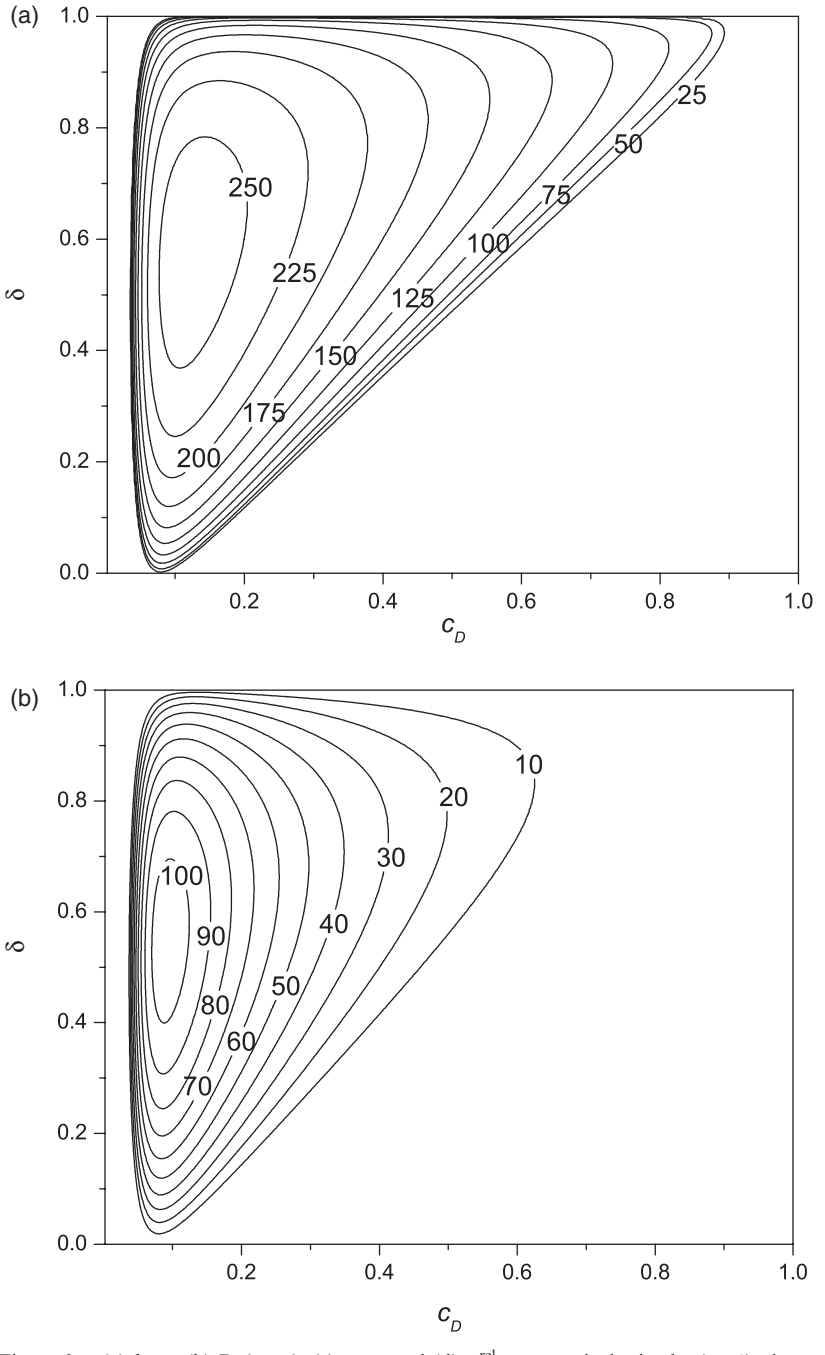

Figure 3. (a) $k_{\max}$, (b) $\mathrm{Re}\{\sigma_{\max}\}$, (c) $\omega_{\max}$ and (d) $\omega_{\max}^{\mathrm{rel}}$, respectively, in the (c_D, δ)-plane.

Figure 3(c) is a contour plot of the (*geostationary*) frequency of the most unstable mode, given by $\omega_{\max}$, in the (c_D, δ)-plane assuming $R_e = 279$ and $\gamma = 2.56$. Comparing figure 3(c) with figure 2(c), the frequencies of the most unstable modes can be as much as 100 times larger than the uncoupled frequencies in the unstable

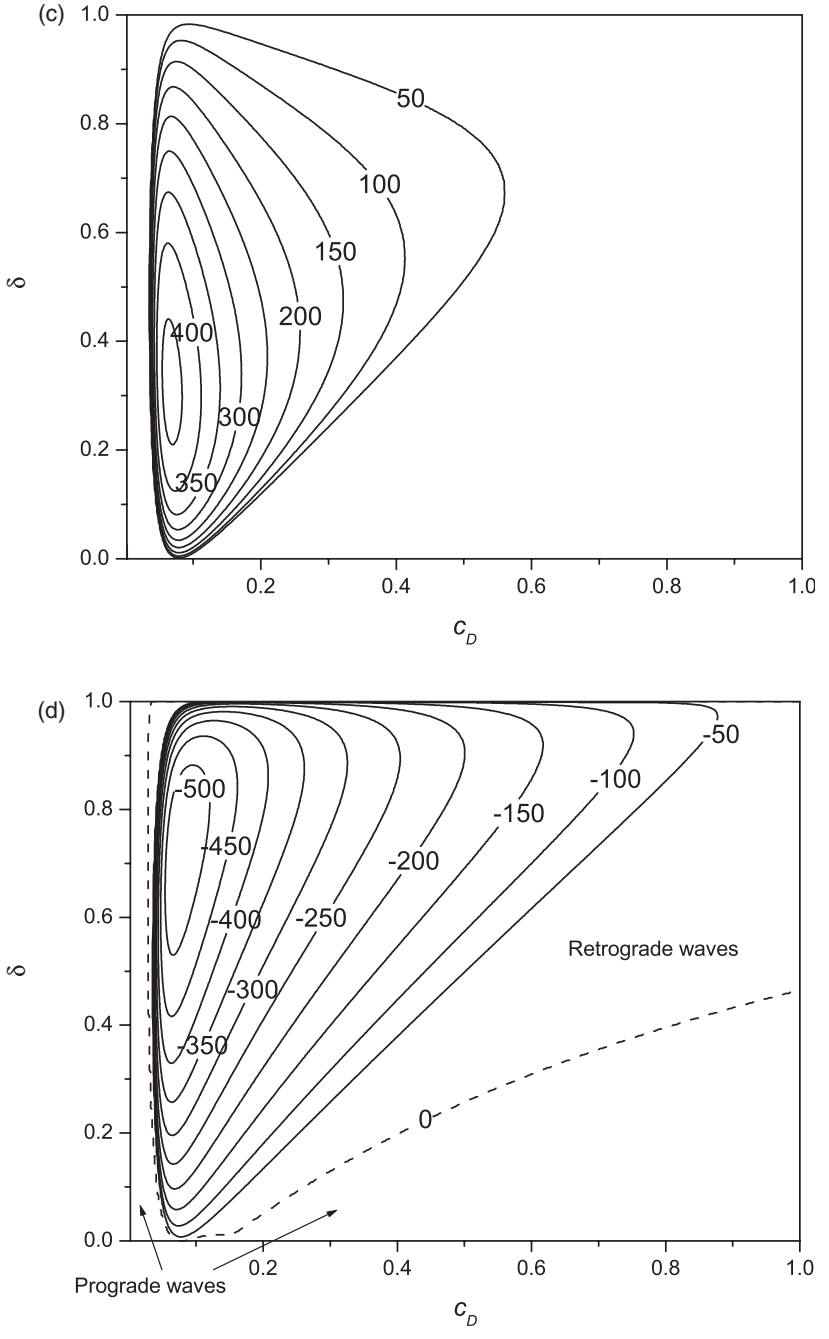

Figure 3. Continued.

region for the same value of c_D. Here again, the trend that $\omega_{\max}$ increases as δ increases initially from zero, with a maximum reached and then decreasing as $\delta \to 1^-$ is seen. The maximum value of $\omega_{\max}$ in figure 3(c) is about 466.50 (corresponding, dimensionally, to a mode with a period of about 7 min) and is located at about

$(c_D, \delta) \simeq (0.12, 0.58)$. For the 'typical' (c_D, δ) values of (0.25, 0.38), as determined in (16), $\omega_{\max} \simeq 206.37$ (corresponding, dimensionally, to a mode with a geostationary period of about 17 min).

Figure 3(d) is a contour plot of the relative frequency of the most unstable mode (in a frame of reference moving with the mean flow) $\omega_{\max}^{\mathrm{rel}}$ in the (c_D, δ)-plane assuming $R_e = 279$ and $\gamma = 2.56$. Unlike the most unstable modes for $\delta = 0$, without and even with rotation included (see figure 2d and Swaters 2003), the coupled modes can propagate retrograde relative to the mean flow (i.e., in the co-moving frame the modal phase velocities can be negative). The trend in figure 3(c) is that $\omega_{\max}$ decreases as δ increases initially from zero (and is initially positive implying prograde propagation), with, generally speaking, a negative minimum reached (implying retrograde propagation) and then increasing as $\delta \to 1^-$. Although it cannot be discerned clearly from figure 3(d), in fact $\omega_{\max}^{\mathrm{rel}}$ is *positive* as $\delta \to 1^-$. The minimum value of $\omega_{\max}^{\mathrm{rel}}$ in figure 3(c) is about -539.24 (corresponding, dimensionally, to a retrograde unstable mode with a co-moving period of about 6.3 min) and is located at about $(c_D, \delta) \simeq (0.08, 0.73)$. For the 'typical' (c_D, δ) values of (0.25, 0.38), as determined in (16), $\omega_{\max}^{\mathrm{rel}} \simeq -182.93$ (corresponding, dimensionally, to a retrograde mode with a co-moving period of about 19 min).

Perhaps the most important property seen in figures 3 is that when full dynamical coupling occurs between the frictionally destabilized abyssal overflow and the overlying internal gravity wave field, the range of c_D values for which instability can occur is much larger than that associated for $\delta = 0$. As can be seen in figure 2, and as follows from (26), when $\delta = 0$, instability can only occur within $0 < c_D < 0.25$. However, figure 3 shows that once $\delta > 0$, instability is possible for $c_D \geq 0.25$, although the growth rates diminish as c_D increases.

In addition, unlike in figure 2 where $k_{\max}$, $\mathrm{Re}(\sigma_{\max})$, $\omega_{\max}$ and $\omega_{\max}^{\mathrm{rel}}$, all monotonically decrease, as c_D increases from zero, from their limiting values associated with $c_D \to 0^+$, in the situation when $0 < \delta < 1$ (as in figure 3), $k_{\max}$, $\mathrm{Re}\{\sigma_{\max}\}$ and $\omega_{\max}$ possess a distinct local maximum, respectively, and $\omega_{\max}^{\mathrm{rel}}$ possesses a distinct local minimum, for a finite nonzero value of c_D. The dependence of the most unstable mode parameters on c_D is shown in figures 4. figures 4(a), (b), (c) and (d) are plots of $k_{\max}$, $\mathrm{Re}\{\sigma_{\max}\}$, $\omega_{\max}$ and $\omega_{\max}^{\mathrm{rel}}$, respectively, for $\delta = 0.38$ (the value listed in (2.16)) *versus* c_D. The specific values of c_D associated with the individual local extreme values for $k_{\max}$, $\mathrm{Re}\{\sigma_{\max}\}$, $\omega_{\max}$ and $\omega_{\max}^{\mathrm{rel}}$, respectively, are not necessarily the same for each modal parameter because of the 'slightly' different explicit and implicit individual dependency on c_D.

Figure 4(b) suggests that the maximum value of $\mathrm{Re}\{\sigma_{\max}\}$ (maximized with respect to c_D) is approximately 98.32 (corresponding, dimensionally, to a mode with an e-folding amplification time of about 5.5 min) and is located at $c_D \simeq 0.09$. It follows from figures 4(a), (c) and (d) that $k_{\max} \simeq 248$, $\omega_{\max} \simeq 436$ and $\omega_{\max}^{\mathrm{rel}} \simeq -402$ for $c_D \simeq 0.09$ (corresponding, dimensionally, to a mode with a wavelength of about 380 m and geostationary and co-moving retrograde periods of, respectively, 7.8 and 8.4 min).

The dependence of the most unstable mode parameters on δ is shown in figures 5. Figures 5(a), (b), (c) and (d) are plots of $k_{\max}$, $\mathrm{Re}\{\sigma_{\max}\}$, $\omega_{\max}$ and $\omega_{\max}^{\mathrm{rel}}$, respectively, for $c_D = 0.25$ (the value listed in (16)) *versus* δ. The parameters $k_{\max}$, $\mathrm{Re}\{\sigma_{\max}\}$ and $\omega_{\max}$ possess a distinct local maximum, respectively, and $\omega_{\max}^{\mathrm{rel}}$ possesses a distinct local minimum, for a finite nonzero value of δ. As before, the specific values of δ

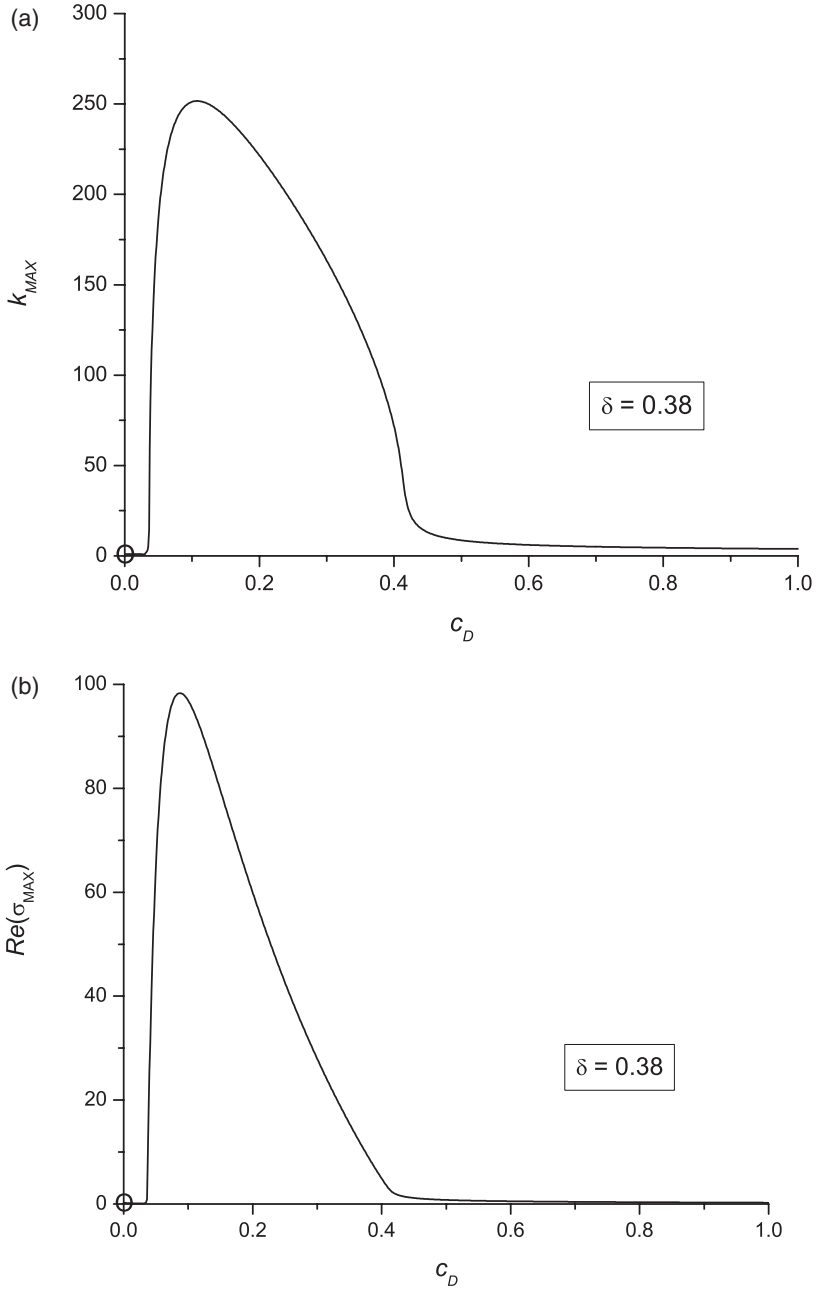

Figure 4. (a) $k_{\max}$, (b) $\mathrm{Re}\{\sigma_{\max}\}$, (c) $\omega_{\max}$ and (d) $\omega_{\max}^{\mathrm{rel}}$, respectively, *vs.* c_D, for $\delta = 0.38$.

associated with each individual local extreme value of $k_{\max}$, $\mathrm{Re}\{\sigma_{\max}\}$, $\omega_{\max}$ and $\omega_{\max}^{\mathrm{rel}}$ are not necessarily the same for each modal parameter because of the ('slightly') different explicit and implicit individual dependency on δ.

Figure 5(b) suggests that the maximum value of $\mathrm{Re}\{\sigma_{\max}\}$ (maximized with respect to δ) is approximately 61.22 (corresponding, dimensionally, to a mode with an e-folding

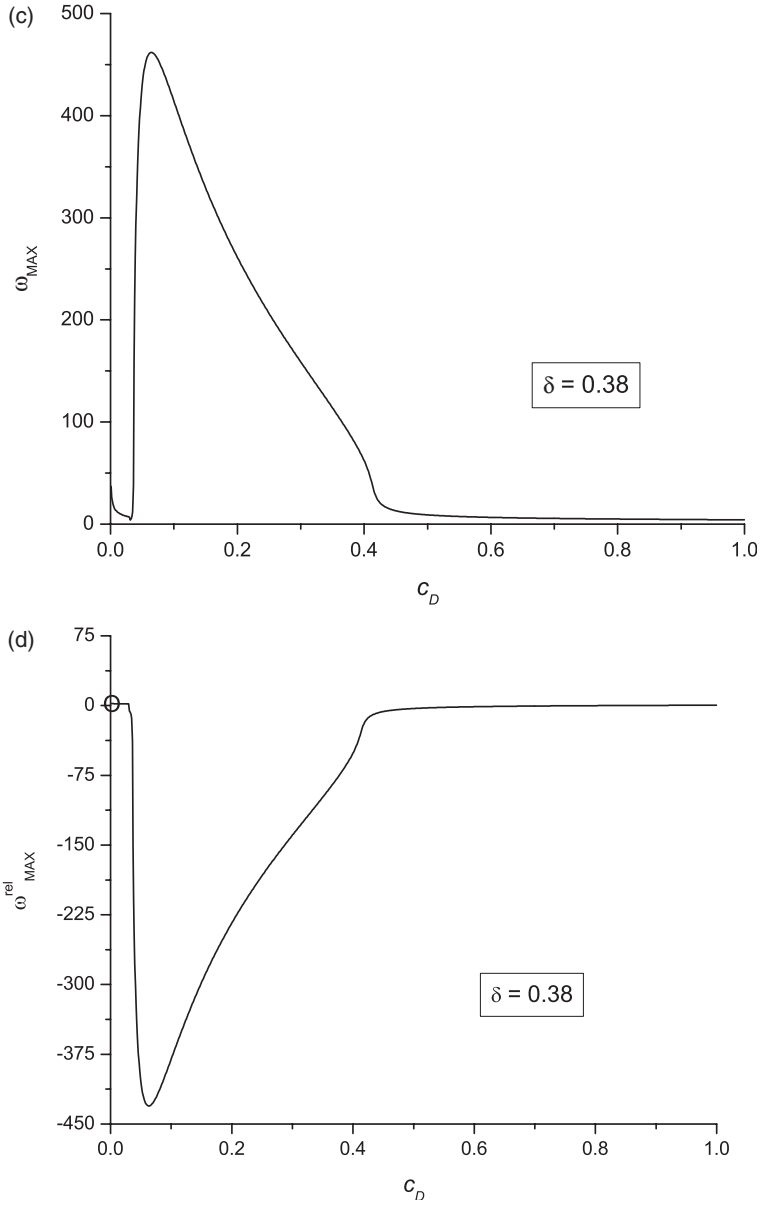

Figure 4. Continued.

amplification time of about 8.8 min) and is located at $\delta \simeq 0.66$ (i.e., $H \simeq 1.52h_*$). It follows from figures 5(a), (c) and (d) that $k_{\max} \simeq 237$, $\omega_{\max} \simeq 163$ and $\omega^{\text{rel}}_{\max} \simeq -309$ for $\delta \simeq 0.66$ (corresponding, dimensionally, to a mode with a wavelength of about 398 m and geostationary and co-moving retrograde periods of, respectively, 21 and 11 min). Perhaps the most important physical implication associated with figure 5 is that the strong dependence of the growth rate, periods and wavelengths on the depth of the overlying water column suggests that the instability described here will intensify in the immediate near-sill region where H is smaller.

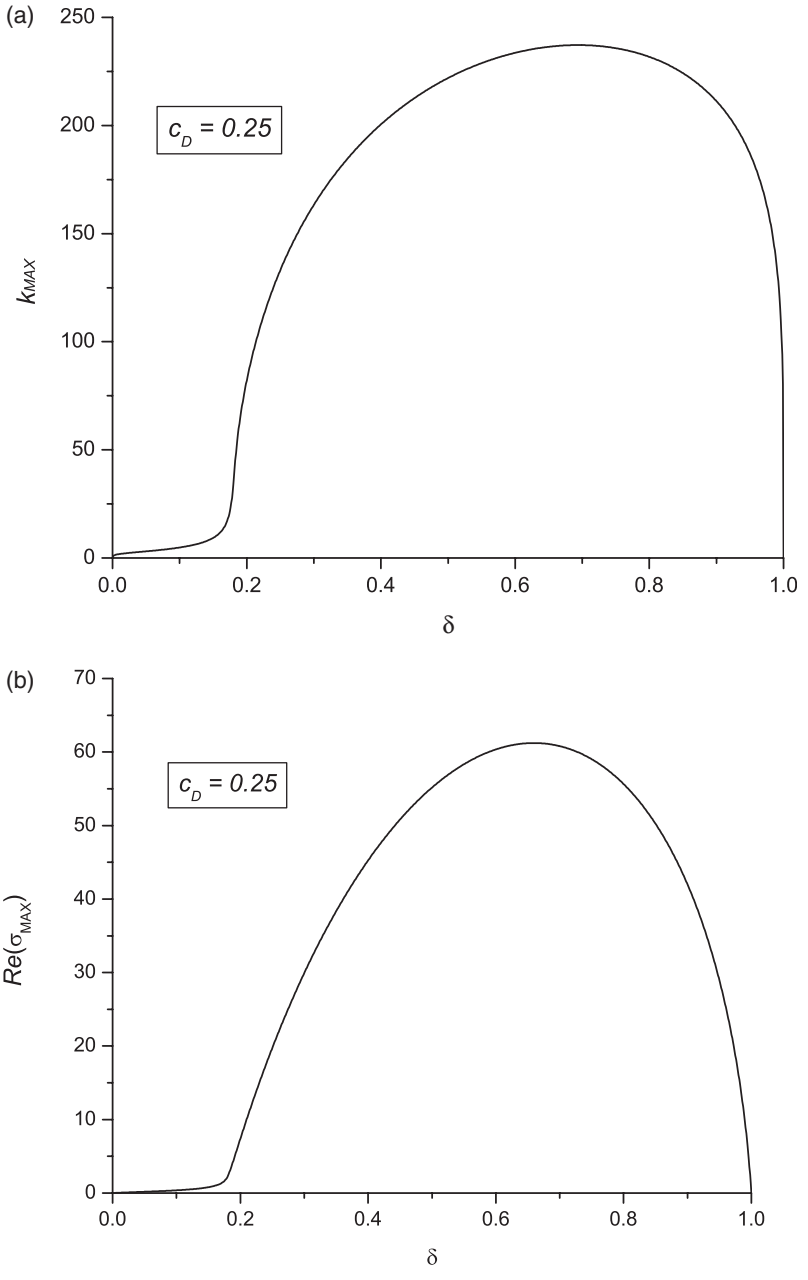

Figure 5. (a) $k_{\max}$, (b) $\mathrm{Re}\{\sigma_{\max}\}$, (c) $\omega_{\max}$ and (d) $\omega_{\max}^{\mathrm{rel}}$, respectively, *vs.* δ, for $c_D = 0.25$.

5. Conclusions

Abyssal overflows in the ocean are a significant source for the formation of deep boundary currents and hence the thermohaline circulation. For example, the DSO is the largest single source for the North Atlantic Deep Water transport (Girton and

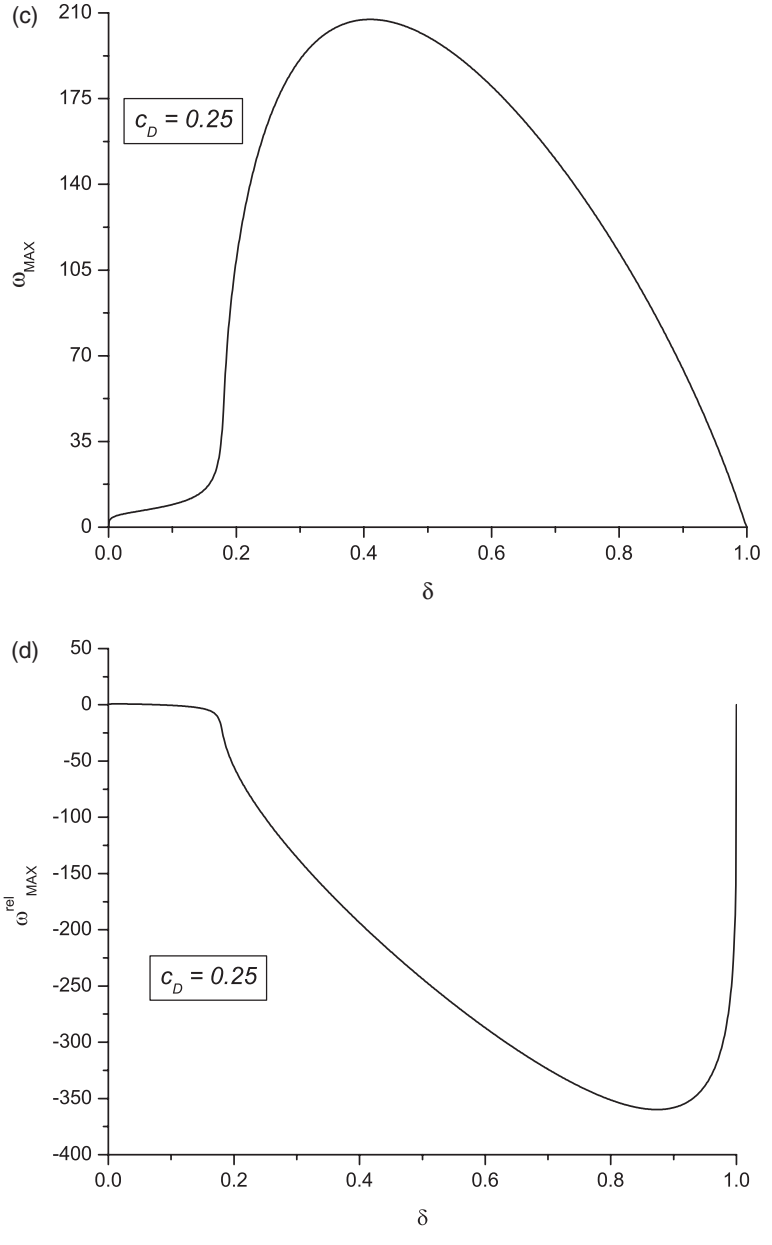

Figure 5. Continued.

Sanford 2003). As these abyssal overflows cross their respective sills, their speeds increase with bottom friction and downslope gravitational acceleration playing a prominent role in the dynamics. The speeds associated with abyssal overflows are observed to exceed the local long gravity wave phase and group speeds. This suggests that abyssal overflows can become supercritical with the possibility of frictional destabilization occurring (the oceanographic analogue of roll wave formation).

Through this particular transition mechanism, it can reasonably be expected that the unstable overflows will dynamically interact with the overlying water column and generate internal gravity waves that in turn interact with the abyssal current. Indeed, a full understanding of the coupling between internal gravity waves and the deep ocean circulation remains an important area of oceanographic research.

In this article, the frictionally induced linear instability of supercritical abyssal overflows that are dynamically coupled to internal gravity waves in the overlying water column has been examined. The stratification characteristics of the $2\frac{1}{2}$-layer model used here have been selected to mimic the mean vertical density profile in the DSO (Girton and Sanford 2003). In particular, it has been shown that the dynamical coupling with ambient internal gravity waves leads to a significant 'up or blue spectrum' shift in the frequencies, wavelengths and growth rates as compared to an instability theory without dynamical coupling (Swaters 2003). For environmental parameter values characteristic of the DSO, the most unstable mode has been found to have a wavelength of about 484 m, an e-folding amplification time of about 13 min, a geostationary period of about 17 min and propagates in a retrograde manner with a co-moving period of about 19 min.

Several general dynamical properties that are particularly noteworthy were described. When dynamical coupling with internal gravity waves is included in the transition to instability model, it was shown that instability occurs for a larger set of bottom friction (or drag) parameter values (and hence Froude numbers) than that known for the uncoupled problem. Moreover, unlike in the uncoupled instability problem, the maximum growth rate with respect to the bottom drag coefficient does not occur for the unphysical value of zero drag (which has an infinite abyssal current velocity associated with it). That is, the maximum growth rate, when dynamical coupling is accounted for, occurs at a discrete finite abyssal overflow velocity.

In addition, it has been shown that the growth rate of the most unstable mode does not depend monotonically on the ratio of the depth of the overlying water column to the mean thickness of the abyssal current. Specifically, it has been shown that the growth rate of the most unstable mode (for a bottom drag coefficient characteristic of the DSO) is maximized when $\delta \equiv h_*/H \simeq 0.66$, which suggests that the growth rate will be largest if the abyssal current is about 528 m thick (based on $H \simeq 800$ m). Alternatively, for the DSO value of $h_* \simeq 300$ m, this conclusion suggests that this mode of transition would be most vigorous where the scale depth of the overlying water column is about $H \simeq 450$ m (i.e., nearer the location of the sill).

There remain interesting questions that need to be answered. The model here is layered. It would be interesting to determine the stability characteristics in a continuously stratified configuration. The possible presence of a mean velocity in the overlying water column has been ignored here. A substantially more challenging and interesting problem would be to determine the stability characteristics of the laminar Cenedese *et al*. (2004) solution. Determining the stability characteristics associated with the KH mode of transition would be interesting notwithstanding the observation by Cenedese *et al*. (2004) that the wave-like disturbances seen in their experiments seem unrelated to this mode of transition. The effect of rotation needs to be properly determined in the coupled situation. Finite-amplitude effects have been completely ignored here. A theory for the nonlinear saturation of the weakly nonlinear instability needs to be developed. In the real ocean, the full transition sequence undoubtedly consists of the frictional destabilization described here, which subsequently evolves

to the point where geostrophic processes become important, which, in turn, leads into full baroclinic instability and cyclogenesis in abyssal overflows (Bruce 1995, Spall and Price 1998, Krauss and Käse 1998 and Reszka *et al*. 2002). Whether or not this viewpoint has any merit can likely only be resolved by full numerical simulations.

Acknowledgements

Preparation of this manuscript was supported in part by Research Grants awarded by the Natural Sciences and Engineering Research Council of Canada.

References

Baines, P.G., *Topographic Effects in Stratified Flows*, 1995 (Cambridge University Press: Cambridge, New York, Melbourne).

Bruce, J.G., Eddies southwest of Denmark Strait. *Deep-Sea Res*., 1995, **42**, 13–29.

Cenedese, C., Whitehead, J.A., Ascarelli, T.A. and Ohiwa, M., A dense current flowing down a sloping bottom in a rotating fluid. *J. Phys. Oceanogr*., 2004, **34**, 188–203.

Dickson, R.R. and Brown, J., The production of North Atlantic Deep Water: sources, rates, and pathways. *J. Geophys. Res*., 1994, **99**, 12319–12341.

Emms, P.W., A streamtube model of rotating turbidity currents. *J. Mar. Res*., 1998, **56**, 41–74.

Etling, D., Gelhardt, F., Schrader, U., Brennecke, F., Kühn, G., Chabert d'Hieres, G. and Didelle, H., Experiments with density currents on a sloping bottom in a rotating fluid. *Dyn. Atmos. Oceans*, 2000, **31**, 139–164.

Girton, J.B. and Sanford, T.B., Synoptic sections of the Denmark Strait overflow. *Geophys. Res. Lett*., 2001, **28**, 1619–1622.

Girton, J.B. and Sanford, T.B., Descent and modification of the Denmark Strait overflow. *J. Phys. Oceanogr*., 2003, **33**, 1351–1364.

Houghton, R.W., Schlitz, R., Beardsley, R.C., Butman, B. and Chamberlin, J.L., The middle Atlantic bight cold pool: evolution of the temperature structure during summer 1979. *J. Phys. Oceanogr*., 1982, **12**, 1019–1029.

Jeffreys, H., The flow of water in an inclined channel of rectangular bottom. *Phil. Mag*., 1925, **49**, 793–807.

Jiang, L. and Garwood, R.W., Three-dimensional simulations of overflows on continental slopes. *J. Oceanogr*., 1996, **26**, 1214–1233.

Jungclaus, J.H., Hauser, J. and Käse, R.H., Cyclogenesis in the Denmark Strait Overflow plume. *J. Phys. Oceanogr*., 2001, **31**, 3214–3228.

Karsten, R.H., Swaters, G.E. and Thomson, R.E., Stability characteristics of deep water replacement in the Strait of Georgia. *J. Phys. Oceanogr*., 1995, **25**, 2391–2403.

Käse, R.H., Girton, J.B. and Sanford, T.B., Structure and variability of the Denmark Strait overflow: model and observations. *J. Geophys. Res*., 2003, **108**(C6), 3181, 10.1029/2002JC001548.

Käse, R.H. and Oschlies, A., Flow through Denmark Strait. *J. Geophys. Res*., 2000, **105**, 28527–28546.

Killworth, P.D., Mixing on the Weddell Sea continental slope. *Deep-Sea Res*., 1977, **24**, 427–448.

Krauss, W. and Käse, R.H., Eddy formation in the Denmark Strait overflow. *J. Geophys. Res*., 1998, **103**, 15523–15538.

Lane-Serff, G.F. and Baines, P.G., Eddy formation by dense flows on slopes in a rotating fluid. *J. Fluid Mech*., 1998, **363**, 229–253.

LeBlond, P.H., Ma, H., Doherty, F. and Pond, S., Deep and intermediate water replacement in the Strait of Georgia. *Atmos.-Ocean*, 1991, **29**, 288–312.

LeBlond, P.H. and Mysak, L.A., *Waves in the Ocean*, 1981 (Elsevier: Amsterdam, Oxford, New York).

Masson, D., Deep water renewal in the Strait of Georgia. *Estuarine, Coastal and Shelf Science*, 2002, **54**, 115–126.

Needham, D.J. and Merkin, J.H., On roll waves down an inclined channel. *Proc. R. Soc. Lond*., 1984, **A394**, 259–278.

Poulin, F.J. and Swaters, G.E., Sub-inertial dynamics of density-driven flows in a continuously stratified fluid on a sloping bottom. I. Model derivation and stability characteristics. *Proc. R. Soc. Lond*., 1991, **A455**, 2281–2304.

Price, J.F. and Baringer, O.M., Outflows and deep water production by marginal seas. *Progr. Oceanogr*., 1994, **33**, 161–200.

Reszka, M.K., Swaters, G.E. and Sutherland, B.R., Instability of abyssal currents in a continuously stratified ocean with bottom topography. *J. Phys. Oceanogr*., 2002, **32**, 3528–3550.
Smith, P.C., A streamtube model for bottom boundary currents in the ocean. *Deep-Sea Res*., 1975, **22**, 853–873.
Spall, M.A. and Price, J.F., Mesoscale variability in Denmark Strait: the PV outflow hypothesis. *J. Phys. Oceanogr*., 1998, **28**, 1598–1623.
Swaters, G.E., On the baroclinic instability of cold-core coupled density fronts on a sloping continental shelf. *J. Fluid Mech*., 1991, **224**, 361–382.
Swaters, G.E., Numerical simulations of the baroclinic dynamics of density-driven coupled fronts and eddies on a sloping bottom. *J. Geophys. Res*., 1998, **103**, 2945–2961.
Swaters, G.E., Baroclinic characteristics of frictionally destabilized abyssal overflows. *J. Fluid Mech*., 2003, **489**, 349–379.
Swaters, G.E., On the meridional flow of source-driven abyssal currents in a stratified basin with topography. Part I. Model development and dynamical characteristics. *J. Phys. Oceanogr*., 2005a (In press).
Swaters, G.E., On the meridional flow of source-driven abyssal currents in a stratified basin with topography. Part II. Numerical simulation. *J. Phys. Oceanogr*., 2005b (In press).
Swaters, G.E. and Flierl, G.R., Dynamics of ventilated coherent cold eddies on a sloping bottom. *J. Fluid Mech*., 1991, **223**, 565–587.
Whitehead, J.A., Stern, M.E., Flierl, G.R. and Klinger, B.A., Experimental observations of baroclinic eddies on a sloping bottom. *J. Geophys. Res*., 1990, **95**, 9585–9610.
Whitham, G.B., *Linear and Nonlinear Waves*, 1974 (Wiley: New York, Chichester, Brisbane, Toronto).
Worthington, L.V., An attempt to measure the volume transport of Norwegian Sea overflow water through the Denmark Strait. *Deep-Sea Res*., 1969, **16**, 421–432.
Worthington, L.V. and Wright, W.R., In *North Atlantic Ocean Atlas*, Vol. II, 1970 (The Woods Hole Oceanographic Institution Atlas Series: Woods Hole, MA).